Journal of Alloys and Compounds 509 (2011) 4805–4810

Contents lists available at ScienceDirect

Journal of Alloys and Compounds

journal homepage: www.elsevier.com/locate/jallcom

Thermodynamic optimization of the boron–cobalt–iron system

Y.Q. Liu [a,*], X.S. Zhao [b], J. Yang [a], J.Y. Shen [b]

[a] School of Materials Science and Technology, China University of Geosciences, Beijing 100083, PR China
[b] Mining, Metallurgy & Materials Research Department, General Research Institute for Nonferrous Metals, Beijing 100088, PR China

ARTICLE INFO

Article history:
Received 28 November 2010
Received in revised form 21 January 2011
Accepted 30 January 2011
Available online 23 February 2011

Keywords:
B–Co–Fe system
CALPHAD
Phase diagrams
Thermodynamic modeling

ABSTRACT

A thermodynamic optimization of the boron–cobalt–iron ternary system is performed based on thermodynamic models of the three constitutional binary systems and the experimental data on phase diagrams and thermodynamic properties of the ternary system. The liquid, fcc_A1, bcc_A2 and hcp_A3 solution phases are described by the substitutional solution model. The three intermediate line compounds, (Co,Fe)B, $(Co,Fe)_2B$ and $(Co,Fe)_3B$, are described by the two sublattice model. A set of thermodynamic parameters are obtained. The calculated phase diagram and thermodynamic properties are in reasonable agreement with most of the experimental data.

1. Introduction

Cobalt–iron–boron alloys are among the important transition metal–boron alloys widely used in the industry owing to their high hardness and resistance to wear. The cobalt–boron, iron–boron and cobalt–iron–boron alloys, characterized by their excellent soft magnetic property, favorable mechanical performance and good corrosion resistance, are promising for technological applications [1]. The cobalt–iron–boron alloys also show large glass forming ability (GFA). Amorphous alloys processed through rapid solidification and nanocrystalline materials derived from the amorphous matrix show special properties of technological interest [2,3]. For example, amorphous iron-cobalt-boron alloys with induced uniaxial anisotropy exhibits high magnetoelastic characteristics, and have potentials to be used as sensitive elements of various mechanical-deformation gages, magnetoelastic transducers, delay lines of sonic and ultrasonic signals [4]. The rapidly solidified iron-transition metal-boron alloys after consolidation and subsequent heat treatment show enhanced mechanical properties at high temperatures [5]. Understanding the phase relations and the thermodynamic properties of the B–Co–Fe system is, thus, of particular interest in identifying alloy compositions and processing methods for obtaining desired properties in these materials. In this study, a thermodynamic optimization of the B–Co–Fe ternary system is carried out using the CALPHAD method based on the thermodynamic descriptions of the three constitutional binary systems and the experimental phase diagram and thermodynamic data.

2. Literature review

2.1. The B–Co system

The B–Co system is characterized by the occurrence of three intermediate compounds, Co_3B, Co_2B and CoB. Boron is slightly soluble in the fcc_A1 Co forming αCo terminal solid solution phase, whereas no Co solubility has been detected in the rhombohedral B (βB) phase. The B–Co system has been thermodynamically modeled by several researchers [6–9]. The calculated results of Ref. [6] show large discrepancies with the current experimentally derived phase diagram and thermodynamic data due to limited experimental information used in the modeling. The thermodynamic assessment of Ref. [7] seems to be unreliable, as pointed out by Du et al. [8], since inaccurate enthalpy of mixing values were used in the optimization. Sixteen parameters were used for the liquid phase in Ref. [9], although most of the experimental data can be successfully reproduced by their model. Du et al. [8] recently reinvestigated the B–Co phase diagram using X-ray diffraction (XRD), optical microscopy (OM), electron probe microanalysis (EPMA) and differential thermal analysis (DTA) and carried out a critical optimization based on their own results and available data. In the present work, the thermodynamic parameters reported by Du et al. [8], which can well reproduce most of the experimental data, were used. The calculated B–Co phase diagram is presented in Fig. 1.

* Corresponding author at: School of Materials Science and Technology, China University of Geosciences, No.29, Xueyuan Road, Beijing 100083, PR China. Tel.: +86 10 82320512; fax: +86 10 82322974.
E-mail address: liuyuqin@cugb.edu.cn (Y.Q. Liu).

0925-8388/$ – see front matter © 2011 Elsevier B.V. All rights reserved.
doi:10.1016/j.jallcom.2011.01.170

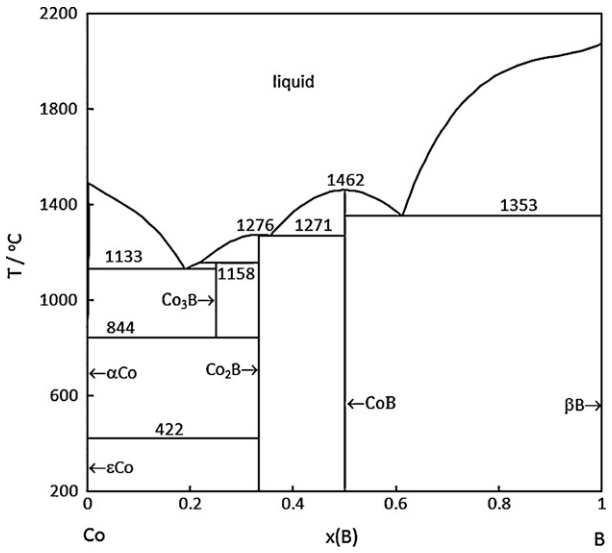

Fig. 1. Calculated B–Co phase diagram based on the thermodynamic description of Du et al. [8].

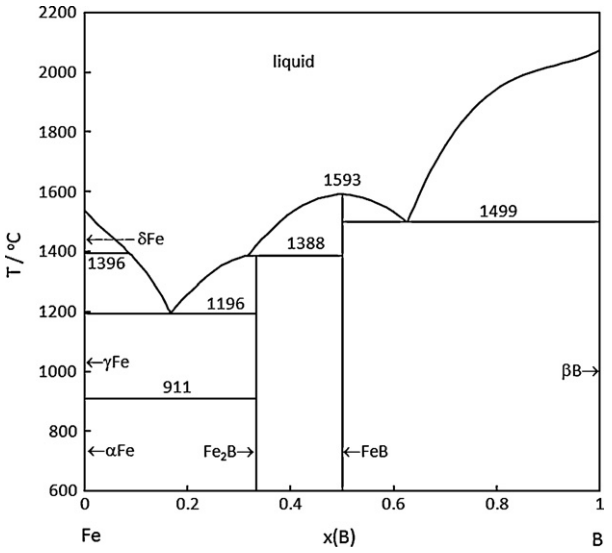

Fig. 2. Calculated B–Fe phase diagram based on the thermodynamic description of Van Rompaey et al. [14].

2.2. The B–Fe system

The equilibrium B–Fe phase diagram is composed of the liquid, bcc_A2 (δFe and αFe solid solution), fcc_A1 (γFe solid solution), rhombohedral B (βB), Fe_2B and FeB phases. Thermodynamic analysis of the B–Fe system has been performed extensively [6,10–15]. Kaufman et al. [6] used the subregular solution model to describe the liquid, bcc_A2 and fcc_A1 phases. Chart [10] provided a six-parameter description for the liquid phase and an estimated solubility of B in the Fe solid solution. In the work of Ohtani et al. [11], the Fe solid solution phases were modeled as interstitial solutions in order to calculate the Fe–B–C ternary phase diagram. Liao and Spear [12] calculated the B–Fe phase diagram assuming no solubility of B in Fe solid solution. The SGTE recommended expressions for the pure elements were not used in the work of [6,10–12]. Hallemans et al. [13] suggested substitutional solubility of B in the Fe and reassessed this system. Van Rompaey et al. [14] developed two sets of thermodynamic descriptions for the B–Fe system, considering B both as interstitial species and as substitutional species in the Fe solid solutions, respectively. More recently, Yoshitomi et al. [15] reassessed the B–Fe system by combining the first principles calculations and CALPHAD method. However, the predicted invariant reaction temperature for liquid ↔ FeB + βB is around 43 °C lower than the widely accepted value of 1500 °C [16]. In the present study, the thermodynamic parameters assessed by Van Rompaey et al. [14], where B was treated as a substitutional species in the Fe solid solution, were adopted. The calculated B–Fe binary phase diagram is shown in Fig. 2.

2.3. The Co–Fe system

The equilibrium phases in the Co–Fe binary system are liquid, bcc_A2 (δFe and α(Fe,Co) solid solution), fcc_A1 (γ(Co,Fe) solid solution), hcp_A3 (εCo solid solution). Fernandez Guillermet [17] carried out a thermodynamic assessment of the Co–Fe system without taking into account the α(bcc_A2)/α′(bcc_B2) order-disorder transition. Colinet and Antoni-Zdziobek [18] modeled this system using a hybrid approach consisting of the cluster variation method (CVM) and CALPHAD assessment, but the effect of ordering on the low-temperature α(bcc_A2)/γ(fcc_A1) equilibrium was not presented. Ohnuma et al. [19] considered the magnetic and chemical ordering contributions of the bcc_B2 structure and reassessed the Fe–Co system based on their own experimental results and available data. The calculated phase diagram showed good agreement with the experimental data. In the present work, thermodynamic parameters assessed by Ohnuma et al. [19] were directly used and the calculated Co–Fe phase diagram is shown in Fig. 3.

2.4. The B–Co–Fe ternary system

The B–Co–Fe ternary system consists of eight equilibrium phases: liquid, bcc_A2 (αFe and δFe solid solution), fcc_A1 (γ(Fe,Co) solid solution), hcp_A3 (εCo solid solution), rhombohedral B (βB), (Co,Fe)B, $(Co,Fe)_2B$ and $(Co,Fe)_3B$. Recently, the experimental phase diagram and thermodynamic data available in the literature were critically reviewed by Fabrichnaya [20]. Key experimental information is briefly discussed below.

Pradelli et al. [21] reported the liquidus surface and the isothermal section at 1000 °C based on XRD, thermal analysis (TA) and OM studies for the concentration range of 0 to 50 at.% B in the B–Co–Fe system. The reported isothermal section at 1000 °C

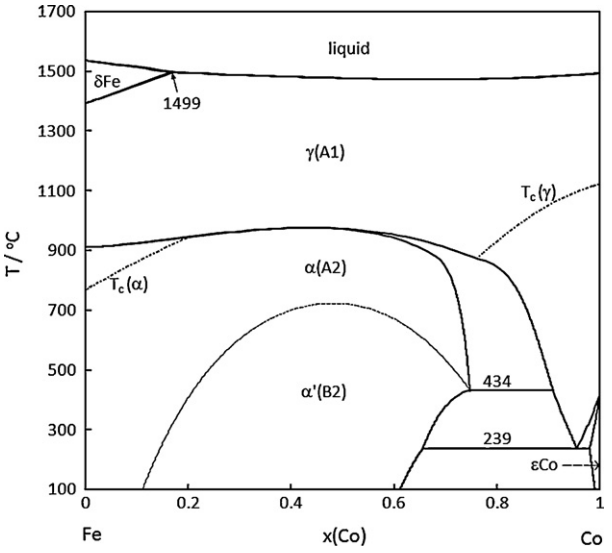

Fig. 3. Calculated Co–Fe phase diagram based on the thermodynamic description of Ohnuma et al. [19].

reasonably agrees with the work of Rogl et al. [22] except for the $(Co,Fe)_3B + (Co,Fe)_2B$ + fcc_A1 three-phase tie-line triangle (see Fig. 7a for details).

van Loo and van Beek [23] measured the partial isothermal section at 1173 K for the concentration range of 0 to 37.5 at.% B using XRD, OM, scanning electron microscopy (SEM) and EPMA. It was revealed that Co_2B and Fe_2B forms continuous solutions $(Co,Fe)_2B$ and Fe can replace large amount of Co in the Co_3B.

The activity of B (referred to pure solid βB) in the ternary B–Co–Fe melt at 1300 °C was determined via the electromotive force (emf) measurements by Ushio and Ogawa [24]. The activity of B was found with negative deviation from ideal solution. Witusiewicz [25] measured the partial enthalpies of formation of the B–Co–Fe melt at 1627 °C by isoperibolic calorimetry.

3. Thermodynamic model

3.1. liquid, fcc_A1, bcc_A2 and hcp_A3 phases

The liquid, fcc_A1, bcc_A2 and hcp_A3 phases are modeled by the substitutional solution model and the Gibbs energy is expressed by Redlich–Kister–Muggianu equation [26],

$$G^{\phi} = x_B^{\phi}\,{}^0G_B^{\phi} + x_{Co}^{\phi}\,{}^0G_{Co}^{\phi} + x_{Fe}^{j}\,{}^0G_{Fe}^{\phi} + RT(x_B^{\phi}\ln x_B^{\phi} + x_{Co}^{\phi}\ln x_{Co}^{\phi} + x_{Fe}^{\phi}\ln x_{Fe}^{\phi}) + x_B^{\phi}x_{Co}^{\phi}L_{B,Co}^{\phi} + x_B^{\phi}x_{Fe}^{\phi}L_{B,Fe}^{\phi} + x_{Co}^{\phi}x_{Fe}^{\phi}L_{Co,Fe}^{\phi} + x_B^{\phi}x_{Co}^{\phi}x_{Fe}^{\phi}L_{B,Co,Fe}^{\phi} + G_{mag}^{\phi} \quad (1)$$

where R is the gas constant and T is the temperature in Kelvin. ϕ represents the liquid, fcc_A1, bcc_A2 and hcp_A3 phases. x_B^{ϕ}, x_{Co}^{ϕ} and x_{Fe}^{ϕ} denote the mole fractions of B, Co and Fe in the ϕ phase, respectively. ${}^0G_B^{\phi}$, ${}^0G_{Co}^{\phi}$ and ${}^0G_{Fe}^{\phi}$ are the molar Gibbs energy of B, Co and Fe with a ϕ structure and taken from the SGTE compilation by Dinsdale [27]. $L_{B,Co}^{\phi}$, $L_{B,Fe}^{\phi}$ and $L_{Co,Fe}^{\phi}$ are the interaction parameters of three constitutional binary systems. $L_{B,Co,Fe}^{\phi}$ is expressed as follows:

$$L_{B,Co,Fe}^{\phi} = x_B\,{}^0L_{B,Co,Fe}^{\phi} + x_{Co}\,{}^1L_{B,Co,Fe}^{\phi} + x_{Fe}\,{}^2L_{B,Co,Fe}^{\phi} \quad (2)$$

where ${}^iL_{B,Co,Fe}^{\phi}(i = 0, 1, 2)$ are the ternary interaction parameters and will be evaluated in this work.

G_{mag}^{ϕ} in Eq. (1) is the magnetic contribution to the Gibbs energy, which vanishes for the liquid phase. For fcc_A1, bcc_A2 and hcp_A3 phases, G_{mag}^{ϕ} is calculated by the Hillert–Jarl–Inden model [28,29]:

$$G_{mag}^{\phi} = RT\,\ln(\beta + 1)g(\tau) \quad (3)$$

where $\tau = T/T_c$, T_c is the Curie temperature, β is the average magnetic moment per atom (in Bohr magnetons). The function $g(\tau)$ is the polynomial derived by Hillert and Jarl [29]. The parameters T_c and β are usually expressed as a function of composition as follows:

$$T_c = x_B \cdot T_{c,B}^0 + x_{Co} \cdot T_{c,Co}^0 + x_{Fe} \cdot T_{c,Fe}^0 + x_B x_{Co} \cdot T_c^{B,Co} + x_B x_{Fe} \cdot T_c^{B,Fe} + x_{Co}x_{Fe} \cdot T_c^{Co,Fe} + x_B x_{Co} x_{Fe} \cdot T_c^{B,Co,Fe} \quad (4)$$

$$\beta_c = x_B \cdot \beta_B^0 + x_{Co} \cdot \beta_{Co}^0 + x_{Fe} \cdot \beta_{Fe}^0 + x_B x_{Co} \cdot \beta^{B,Co} + x_B x_{Fe} \cdot \beta^{B,Fe} + x_{Co}x_{Fe} \cdot \beta^{Co,Fe} + x_B x_{Co} x_{Fe} \cdot \beta^{B,Co,Fe} \quad (5)$$

where $T_{c,i}^0$ and β_i^0 are the Curie temperature and the Bohr magnetons of components i (i = B, Co, Fe), respectively. $T_c^{i,j}$ and $\beta^{i,j}$ are the interaction parameters for the three constitutional binary systems B–Co, B–Fe and Co–Fe. $T_c^{B,Co,Fe}$ and $\beta^{B,Co,Fe}$ are the ternary interaction parameters and are assumed to be zero in this work due to lack of experimental data.

3.2. Line compounds (Co,Fe)B, $(Co,Fe)_2B$ and $(Co,Fe)_3B$

In the B–Co–Fe ternary system, CoB and FeB phases extend at a constant stoichiometry of boron and form line compounds (Co,Fe)B; and Co_2B and Fe_2B phases form line compounds $(Co,Fe)_2B$. The Co_3B phase is stable only in the B–Co binary system and Fe can substitute quite remarkable amount of Co to form $(Co,Fe)_3B$. In this work, these three line compounds are described by two-sublattice model $(Co,Fe)_m(B)_n$. The Gibbs energy of these compounds is expressed by,

$$G^{\varphi} = y'_{Co}\,{}^0G_{Co:B}^{\varphi} + y'_{Fe}\,{}^0G_{Fe:B}^{\varphi} + mRT(y'_{Co}\ln y'_{Co} + y'_{Fe}\ln y'_{Fe}) + y'_{Co}y'_{Fe}\sum_{i=0}^{n} {}^iL_{Co,Fe:B}^{\varphi}(y'_{Co} - y'_{Fe})^i \quad (6)$$

where y'_{Co} and y'_{Fe} are the site fractions of Co and Fe in the first sublattice. ${}^0G_{Co:B}^{\varphi}$ and ${}^0G_{Fe:B}^{\varphi}$ are the Gibbs energy of the end members $(Co)_m(B)_n$ and $(Fe)_m(B)_n$, respectively. ${}^0G_{Co:B}^{\varphi}$ for (Co,Fe)B, $(Co,Fe)_2B$ and $(Co,Fe)_3B$ phases are taken from the binary B–Co system. ${}^0G_{Fe:B}^{\varphi}$ for (Co,Fe)B and $(Co,Fe)_2B$ are taken from the binary B–Fe system. ${}^iL_{Co,Fe:B}^{\varphi}$ is the ith interaction parameter between Co and Fe in the first sublattice and is obtained in the optimization of this work together with ${}^0G_{Fe:B}^{(Co,Fe)3B}$. More detailed description of the sublattice model can be found in Ref. [30].

It is worth to have a short discussion on the magnetic contribution in the (Co,Fe)B, $(Co,Fe)_2B$ and $(Co,Fe)_3B$ phases here. Van Rompaey et al. [14] included the magnetic contribution in iron borides. The Curie temperatures for FeB and Fe_2B obtained in Ref. [14] are 600 K and 1018 K, respectively, which are in good agreement with the experimental values of 598 K for FeB and 1015 K for Fe_2B [31]. Du et al. [8] did not consider the magnetic contribution in the cobalt borides probably due to lack of experimental indication of magnetic transitions. Further experiments are needed to clarify the magnetic transitions in cobalt borides and cobalt-iron borides. In this work, the magnetic contribution to the Gibbs energy for the cobalt borides and cobalt-iron borides are assumed to be zero.

4. Results and discussions

Thermodynamic optimization of the B–Co–Fe ternary system was performed using the PanOptimizer program in the Pandat software [32]. During the optimization process, each piece of experimental data is given a certain weight. The weights were systematically changed during the assessment until most of the experimental data were accounted for within the claimed uncertainty limits. Table 1 presents the summary of the thermodynamic parameters in the B–Co–Fe system.

Fig. 4a presents the calculated liquidus projection along with the isothermal contours at different temperatures. The experimental results of Pradelli et al. [21] are redrawn in Fig. 4b for comparison. The agreement between calculated and experimentally obtained liquidus projection is generally satisfactory. The predicted primary crystallization fields for $(Co,Fe)_3B$ phase is narrower than that experimentally determined [21]. This difference may be traced to the primary crystallization fields of Co_3B in the evaluated B–Co phase diagram, which is much narrower than that reported in Ref. [21]. The ternary eutectic reaction $L \leftrightarrow (Co,Fe)_2B + (Co,Fe)_3B$ + fcc_A1 is well reproduced with the calculated invariant temperature of 1040.7 °C and liquid composition of 20 at.% B and 49 at.% Co, while the experimental determined values are 1040 °C and liquid composition of 20 at.% B and 50 at.% Co.

The calculated activities of B referred to βB in the B–Co–Fe melt at 1300 °C are plotted in Fig. 5 along with the experimental data [24]. The predicted activities of boron agree reasonably with the

Table 1
Summary of the thermodynamic parameters in the B–Co–Fe system.[a]

Phase and thermodynamic parameters	Reference
Liquid: $(B,Co,Fe)_1$	
${}^0L^{liquid}_{B,Co} = -162,096.49 + 48.363T$	[8]
${}^1L^{liquid}_{B,Co} = -2542.75 + 4.712T$	[8]
${}^2L^{liquid}_{B,Co} = 32,123.74$	[8]
${}^0L^{liquid}_{B,Fe} = -126,220 + 29.440T$	[14]
${}^1L^{liquid}_{B,Fe} = 8390$	[14]
${}^2L^{liquid}_{B,Fe} = 33,538$	[14]
${}^0L^{liquid}_{Co,Fe} = -9753.82$	[19]
${}^2L^{liquid}_{Co,Fe} = 2757.96$	[19]
${}^0L^{liquid}_{B,Co,Fe} = -208,172 + 16.8287T$	This work
${}^1L^{liquid}_{B,Co,Fe} = 245,290 - 127.651T$	This work
${}^2L^{liquid}_{B,Co,Fe} = 245,290 - 127.651T$	This work
bcc_A2: $(B,Co,Fe)_1$	
${}^0L^{bcc\_A2}_{B,Fe} = -63,789 + 55.341T$	[14]
${}^0L^{bcc\_A2}_{Co,Fe} = -26,222.7 + 125T - 15.502T\ln T - 632,250T^{-1}$	[19]
${}^2L^{bcc\_A2}_{Co,Fe} = 2686.79 + 632,250T^{-1}$	[19]
${}^0Tc^{bcc\_A2}_{Co,Fe} = 590$	[19]
${}^0\beta^{bcc\_A2}_{Co,Fe} = 1.406 \quad {}^1\beta^{bcc\_A2}_{Co,Fe} = -0.6617$	[19]
fcc_A1: $(B,Co,Fe)_1$	
${}^0L^{fcc\_A1}_{B,Co} = -18,734.7$	[8]
${}^0L^{fcc\_A1}_{B,Fe} = -70,178 + 55.470T$	[14]
${}^0L^{fcc\_A1}_{Co,Fe} = -8968.75$	[19]
${}^2L^{fcc\_A1}_{Co,Fe} = 3528.8$	[19]
${}^0Tc^{fcc\_A1}_{Co,Fe} = 283 \quad {}^1Tc^{fcc\_A1}_{Co,Fe} = 879$	[19]
${}^0\beta^{fcc\_A1}_{Co,Fe} = 8.407 \quad {}^1\beta^{fcc\_A1}_{Co,Fe} = -3.644$	[19]
${}^0L^{fcc\_A1}_{B,Co,Fe} = -77,346.8$	This work
hcp_A3: $(B,Co,Fe)_1$	
${}^0L^{hcp\_A3}_{Co,Fe} = 5000$	[19]
${}^0Tc^{hcp\_A3}_{Co,Fe} = -253 \quad {}^1Tc^{hcp\_A3}_{Co,Fe} = 1494$	[19]
${}^0\beta^{hcp\_A3}_{Co,Fe} = 5.41 \quad {}^1\beta^{hcp\_A3}_{Co,Fe} = -0.24$	[19]
$(Co,Fe)B$: $(Co,Fe)_{0.5}(B)_{0.5}$	
${}^0G^{(Co,Fe)B}_{Co:B} = -40,617 + 134.822T - 21.326T\ln T - 0.00419T^2 + 297,858T^{-1}$	[8]
${}^0G^{(Co,Fe)B}_{Fe:B} = -46,832 + 162.147T - 25.000T\ln T - 0.00250T^2 + 265,000T^{-1}$	[14]
${}^0Tc^{(Co,Fe)B}_{Fe:B} = 600$	[14]
${}^0\beta^{(Co,Fe)B}_{Fe:B} = 1.03$	[14]
${}^0L^{(Co,Fe)B}_{Co,Fe:B} = -1000 - 3.512T$	This work
$(Co,Fe)_2B$: $(Co,Fe)_{0.6667}(B)_{0.3333}$	
${}^0G^{(Co,Fe)2B}_{Co:B} - 0.6667{}^0G^{hcp\_A3}_{Co} - 0.3333{}^0G^{\beta B}_{B} = -28,564 + 5.077T$	[8]
${}^0G^{(Co,Fe)2B}_{Fe:B} = -32,029 + 160.620T - 26.350T\ln T - 0.00236T^2 + 243,997T^{-1}$	[14]
${}^0Tc^{(Co,Fe)2B}_{Fe:B} = 1018$	[14]
${}^0\beta^{(Co,Fe)2B}_{Fe:B} = 1.91$	[14]
${}^0L^{(Co,Fe)2B}_{Co,Fe:B} = -20,271.21 + 15.000T$	This work
${}^1L^{(Co,Fe)2B}_{Co,Fe:B} = -3237.94 + 5.000T$	This work
$(Co,Fe)_3B$: $(Co,Fe)_{0.75}(B)_{0.25}$	
${}^0G^{(Co,Fe)3B}_{Co:B} - 0.75{}^0G^{hcp\_A3}_{Co} - 0.25{}^0G^{\beta B}_{B} = -21,131.79 + 3.1928T$	[8]
${}^0G^{(Co,Fe)3B}_{Fe:B} - 0.75{}^0G^{bcc\_A2}_{Fe} - 0.25{}^0G^{\beta B}_{B} = -20,080 + 3.712T$	This work
${}^0L^{(Co,Fe)3B}_{Co,Fe:B} = -42,300.34 + 30T$	This work

[a] Temperature (T) in Kelvin and Gibbs energy in J/mol-atom.

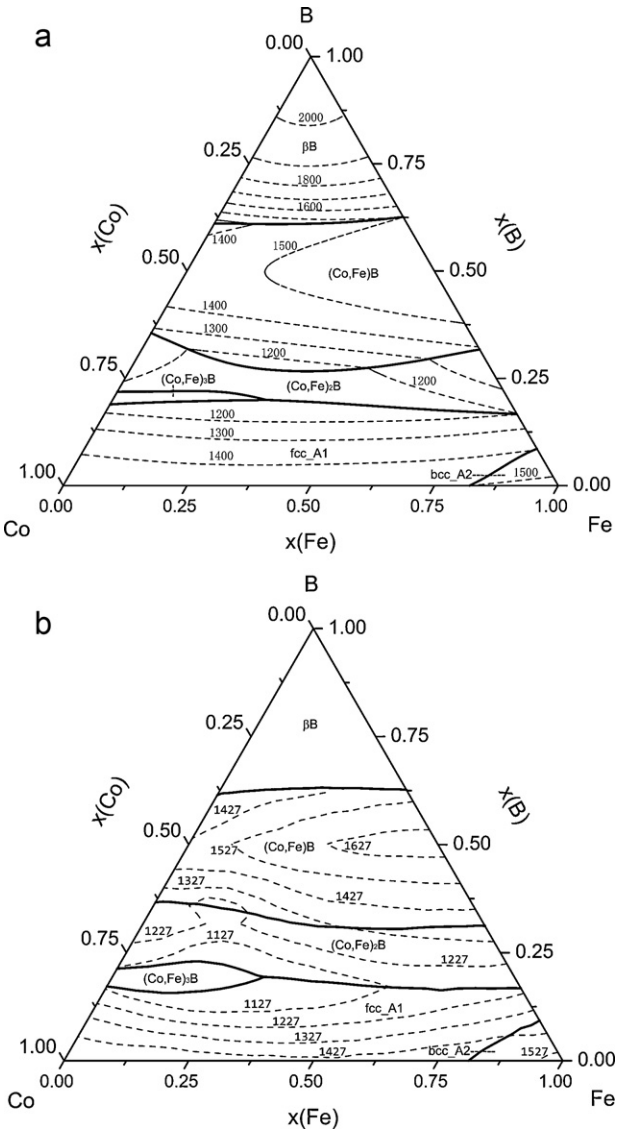

Fig. 4. (a) Calculated liquidus projection of the B–Co–Fe system along with the isothermal contours at different temperatures and (b) the experimentally determined B–Co–Fe liquidus projection by Pradelli et al. [21].

experimental results. The predicted activities of B show large negative deviation from the ideal solution. At the fixed B content, the activity of B changes slightly with the changes of Co content in the single-phase liquid region.

Fig. 6 presents the calculated enthalpies of mixing for the B–Co–Fe melt at 1627 °C along the lines of $(Fe_{0.25}Co_{0.75})_{1-x}B_x$, $(Fe_{0.5}Co_{0.5})_{1-x}B_x$ and $(Fe_{0.75}Co_{0.25})_{1-x}B_x$. The reference state is liquid B, Co and Fe. The experimental data determined by Witusiewicz [25] are superimposed for comparison. The experimental values are well reproduced by this calculation with an error less than ±2 kJ/mol-atom. At the fixed Fe:Co ratio, the calculated enthalpy of mixing increases in magnitude with the increase in B concentration. The influence of Fe:Co ratio on the enthalpy of mixing is relatively obvious at the high B concentration.

Fig. 7a and b presents the calculated isothermal sections at 1000 °C and 900 °C, respectively. The experimental data are superimposed as dotted lines for comparison. It is evident that CoB and FeB forms continuous solid solutions (Co,Fe)B, while Co_2B and Fe_2B forms continuous solid solutions $(Co,Fe)_2B$. In the $(Co,Fe)_3B$ phase, Fe can substitute up to 41.4 at.% Co at 1000 °C and 55.8 at.% Co at 900 °C, respectively, which is consistent with the experimental data

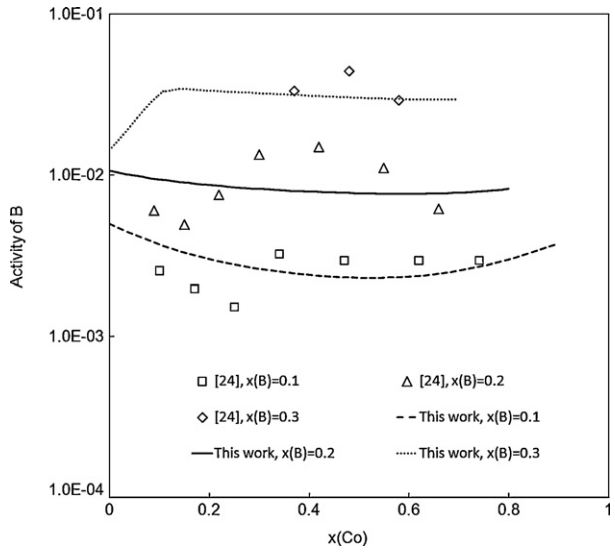

Fig. 5. Calculated activities of B in the B–Co–Fe melt at 1300 °C compared with available experimental data [24]. The reference state is rhombohedral B (βB).

[22,23]. The predicted tie triangle for fcc_A1 + bcc_A2 + $(Co,Fe)_3B$ and bcc_A2 + $(Co,Fe)_3B$ + $(Co,Fe)_2B$ three phase equilibrium is consistent with that determined by van Loo and van Beek [23]. The predicted tie triangle for $(Co,Fe)_3B$ + $(Co,Fe)_2B$ + fcc_A1 three phase equilibrium at 1000 °C agree well with the result of Rogl et al. [22]. The position of tie triangle for $(Co,Fe)_3B$ + $(Co,Fe)_2B$ + fcc_A1 three phase equilibrium reported in Ref. [21] seems to be unreliable as it differs greatly from that reported in Ref. [22] and the trend of tie triangle at 900 °C determined by van Loo and van Beek [23]. In addition, Pradelli et al. [21] reported the composition of liquid for invariant reaction L ↔ $(Co,Fe)_2B$ + $(Co,Fe)_3B$ + fcc_A1 at the invariant temperature 1040 °C is 20 at.% B and 50 at.% Co, which is far outside the $(Co,Fe)_3B$ + $(Co,Fe)_2B$ + fcc_A1 three phase region at 1000 °C reported in the same work and is unlikely to happen. Further experiments are needed to clarify this contradiction.

The calculated quasibinary CoB–FeB phase diagram is plotted in Fig. 8 along with the results of Pradelli et al. [21]. This is a

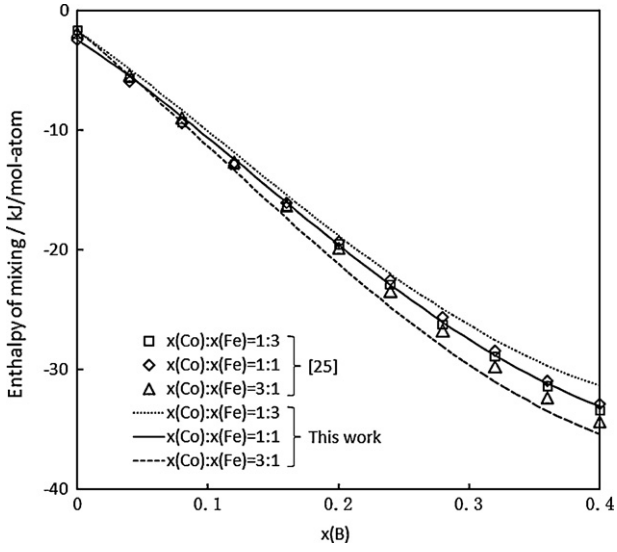

Fig. 6. Predicted enthalpy of formation referred to liquid components for the B–Co–Fe melt at 1627 °C compared with the experimental data [25].

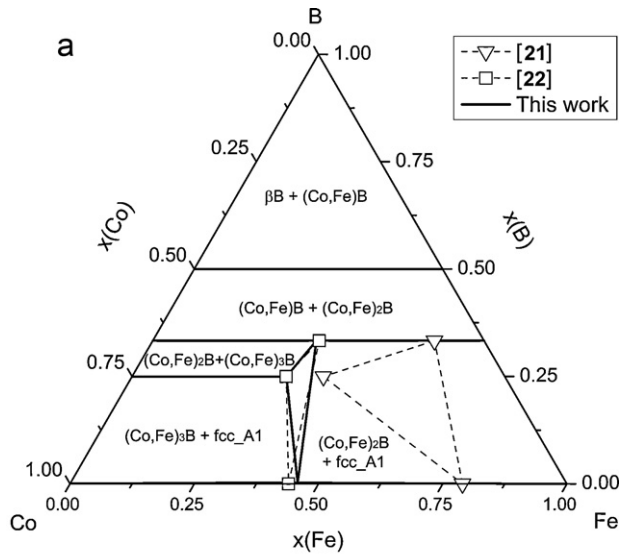

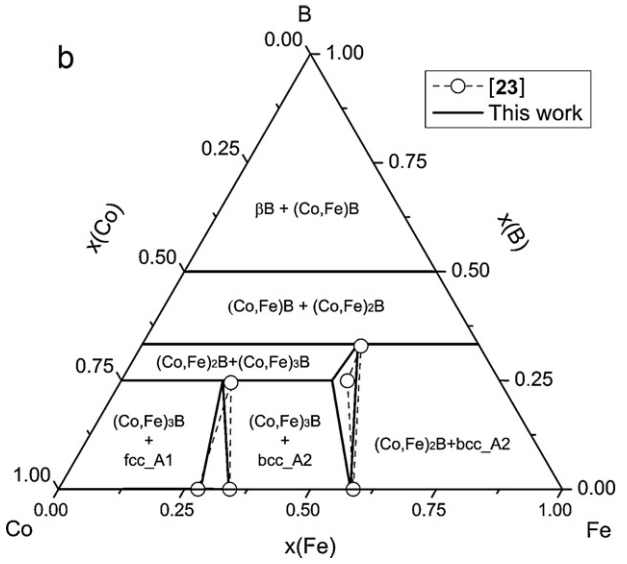

Fig. 7. Calculated isothermal section of the B–Co–Fe system at (a) 1000 °C and (b) 900 °C. The experimental data from Refs. [21–23] are superimposed for comparison.

simple isomorphous system in which there is mutual solubility of the two components, CoB and FeB, in both liquid and solid states throughout the entire composition range. The predicted CoB–FeB phase diagram differs greatly from the experimental result of Pradelli et al. [21]. This discrepancy can be explained from two aspects. The first aspect is the melting point of FeB as reported by [21] is around 57 °C higher than that evaluated by Van Rompaey et al. [14] in the B–Fe binary system. It should be noted that the experimentally determined melting point for FeB differ greatly, from 1540 °C reported by Voroshnin et al. [33] and 1590 °C by Sidorenko et al. [34] to 1650 °C reported by Portnoi et al. [35]. The second aspect is related to the broadness of the liquid + (Co,Fe)B two phase field. For a simple isomorphous system, the existence of such broad two phase field is unlikely when the difference in the enthalpies of fusion of the two terminal constituents are not very large. The respective enthalpies of fusion of CoB and FeB are 26.6 kJ/mol-atom and 33.5 kJ/mol-atom at their melting points.

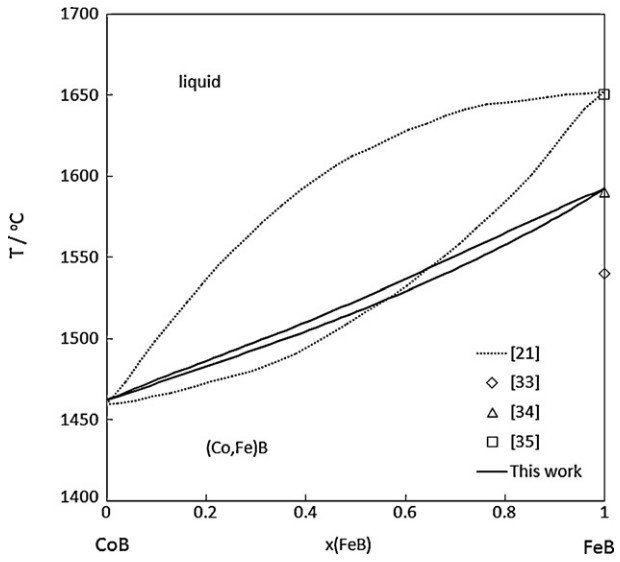

Fig. 8. Predicted quasibinary CoB–FeB phase diagram along with the result of Pradelli et al. [21].

5. Conclusions

A thermodynamic optimization of the B–Co–Fe ternary system has been carried out based on available experimental data. The thermodynamic descriptions of the three constitutional binary systems are taken from previous studies. For the B–Co–Fe ternary system, the substitutional solution model was used to describe the solution phases, while the sublattice model was used for the line compounds (Co,Fe)B, $(Co,Fe)_2B$ and $(Co,Fe)_3B$. A set of thermodynamic parameters have been obtained. The calculated phase diagram and thermodynamic properties are in reasonable agreement with most of the experimental data. Further experiments are needed to clarify the conflicts in the experimentally determined phase diagrams.

Acknowledgements

This project is supported by National Natural Science Foundation of China (Grant No. 51071142) and Scientific Research Foundation for the Returned Overseas Chinese Scholars, State Education Ministry of China. The authors would like to thank CompuTherm LLC for providing the Pandat software.

References

[1] H. Hauser, R. Grössinger, J. Appl. Phys. 85 (1999) 5133.
[2] A. Gupta, K. Ruwali, N. Paul, P. Duhaj, Mater. Sci. Eng. A 304–306 (2001) 371.
[3] K. Kristiakova, P. Svec, Phys. Rev. B 64 (2001) 184202.
[4] A.A. Gavrilyuk, A.L. Semenov, A.V. Semirov, A.V. Gavrilyuk, B.V. Gavrilyuk, N.V. Turik, V.O. Kudryavtsev, Phys. Met. Metallogr. 107 (2009) 18.
[5] L.-M. Pan, N. Saunders, A.P. Miodownik, J. Phase Equilib. 13 (1997) 377.
[6] L. Kaufman, B. Uhrenius, D. Birnie, K. Taylor, CALPHAD 8 (1984) 25.
[7] P.K. Liao, K.E. Spear, Bull. Alloy Phase Diagrams 9 (1988) 452.
[8] Y. Du, J.C. Schuster, Y.A. Chang, Z. Jin, B. Huang, Z. Metallkd. 93 (2002) 1157.
[9] B.V. Mikhailovskii, V.I. Goryacheva, I.B. Kutsenok, Russ. J. Phys. Chem. 73 (1999) 667.
[10] T.G. Chart, Comm. Comm. Eur. (1981), CECA No. 7210-CA/3/303.
[11] H. Ohtani, M. Hasebe, K. Ishida, T. Nishizawa, Trans. Iron Steel Inst. Jpn. 28 (1988) 1043.
[12] P.K. Liao, K.E. Spear, in: H. Okamoto (Ed.), Phase Diagrams of Binary Iron Alloys, ASM Int., Metals Park, OH, 1993, p. 41.
[13] B. Hallemans, P. Wollants, J.R. Roos, Z. Metallkd. 85 (1994) 676.
[14] T. Van Rompaey, K.C. Hari Kumar, P. Wollants, J. Alloys Compd. 334 (2002) 173.
[15] K. Yoshitomi, Y. Nakama, H. Ohtani, M. Haeebe, ISIJ Int. 48 (2008) 835.
[16] T.B. Massalski, H. Okamoto, P.R. Subramanian, L. Kacprzak, Binary Alloys Phase Diagrams, 2nd edition, ASM International, Metals Park, OH, 1990.
[17] A. Fernandez Guillermet, High Temp. High Press. 19 (1987) 477.
[18] C. Colinet, A. Antoni-Zdziobek, JOM 52 (7) (2000) 26.
[19] I. Ohnuma, H. Enoki, O. Ikeda, R. Kainuma, H. Ohtani, B. Sundman, K. Ishida, Acta Mater. 50 (2002) 379.
[20] O. Fabrichnaya, Landolt–Börnstein—Group IV Physical Chemistry, Springer, 2008, p. 379.
[21] G. Pradelli, C. Gianoglio, E. Quadrini, Metall. Ital. 73 (7–8) (1981) 351.
[22] P. Rogl, J.C. Schuster, H. Nowotny, Phase equilibrium and compound formation in Fe–M(metal)–B–X(nonmetal) systems, in: Boron in Steel Proceeding of the International Symposium, Metallurgical Society of AIME, Milwaukee, 1979, p. 33.
[23] F.J.J. van Loo, J.A. van Beek, Z. Metallkd. 80 (1989) 245.
[24] R. Ushio, O. Ogawa, Metall. Trans. B 22B (1991) 47.
[25] V.T. Witusiewicz, Thermochim. Acta 264 (1995) 41.
[26] Y.M. Muggianu, M. Gambino, J.P. Bros, J. Chim. Phys. 22 (1975) 83.
[27] A.T. Dinsdale, CALPHAD 15 (1991) 317.
[28] G. Inden, Proc. Project Meeting, Calphad V, Max-Planck Institute for Metal Research, Dusseldorf, 1976, p. 1.
[29] M. Hillert, M. Jarl, CALPHAD 2 (1978) 227.
[30] I. Ansara, N. Dupin, H.L. Lukas, B. Sundman, in: P. Nash, B. Sundman (Eds.), Proc of TMS Conf on Applications of Thermodynamics in the Synthesis and Processing of Materials, Warrendale, PA, 1995, p. 273.
[31] C.L. Chien, D. Musser, Phys. Rev. B 20 (1979) 283.
[32] S.L. Chen, S. Daniel, F. Zhang, Y.A. Chang, X.Y. Yan, F.Y. Xie, R. Schmid-Fetzer, W.A. Oates, CALPHAD 26 (2002) 175.
[33] L.G. Voroshnin, L.S. Lyakhovich, G.G. Panich, G.F. Protasevish, Met. Sci. Heat Treat. 9 (1970) 732.
[34] F.A. Sidorenko, N.N. Serebrennikov, V.D. Budozhanov, Yu.V. Putintsev, S.N. Trushevskii, V.D. Korabanova, P.V. Gel'd, High Temp. 15 (1977) 36.
[35] K.I. Portnoi, M.Kh. Levinskaya, V.M. Romashov, Sov. Powder Metall. Met. Ceram. 8 (1969) 657.